Available online at www.sciencedirect.com
SCIENCE DIRECT®
Journal of Molecular Catalysis A: Chemical 225 (2005) 1–6
JOURNAL OF MOLECULAR CATALYSIS A: CHEMICAL
www.elsevier.com/locate/molcata

# Chemical and catalytic activity of copper nanoparticles prepared via metal vapor synthesis

Aldo A. Ponce, Kenneth J. Klabunde*

*Department of Chemistry, Kansas State University, Manhattan, KS 66506, USA*

Received 25 March 2004
Available online 1 Ocotber 2004

**Abstract**

Nanocrystalline particles of copper have been prepared using the solvated metal atom dispersion (SMAD) technique. Their chemical and catalytic reactivity have been tested in the Ullman reaction (aryl homocoupling) and the hydrogenation of $CO_2$ to form $CH_3OH$. The powders obtained from different solvents have surface areas of 24–30 $m^2/g$, particle sizes of 20–45 nm, and crystallite sizes of 8–12 nm. The order of activity found toward the aryl homocoupling reaction is $Cu^*$/toluene > $Cu^*$/THF > $Cu^*$/pentane > $Cu^*$/diglyme, with a maximum biphenyl yield of 90% at 150 °C after 6 h for the $Cu^*$/toluene sample. For the $CO_2$ to $CH_3OH$ reaction, a maximum conversion of 80% was obtained for the $Cu^*$/pentane/NC-ZnO sample. In general, the $Cu^*$/nanocrystalline (NC)-ZnO samples show a larger conversion of $CO_2$ to methanol at 450 °C compared with NC-ZnO and NC-ZnO/CuO.


*Keywords:* Hydrogenation; Nanocrystalline; SMAD technique

## 1. Introduction

Metallic nanoparticles have received significant attention by researchers due to their unique properties, different from those of atomic or molecular species and bulk metal. Properties such as color, conductivity, melting point, magnetism, specific heat, and light absorption are often found to be unusual for nanoscale material [1].

There are many approaches to the preparation of ligand-stabilized or ligand-free copper nanoparticles such as: thermal and sonochemical reduction [2–4], chemical reduction [5–9], radiolitic reduction [10], photolysis [11], metal vapor synthesis [12–14], and spray pyrolysis [15].

The reactivity of metallic nanoparticles depends mainly on electronic effects, as the electron density at the active sites (on the surface) can vary due to particle size. This effect is closely related to particle shape and the number of low coordination sites (edges and corners) on the surface [1,14].

Metal nanoparticles are reactive enough that they can be considered as new reagents for organic and organometallic synthesis directly from the metal. These reactions exhibit faster kinetics and often can be carried out at lower temperatures. Copper nanoparticles have been used, for example in: oxidation of phenol with molecular oxygen [12], oxidation of alkanethiols [11], coupling of epoxyalkyl halides [16], and in the Ullman reaction [2,5,6,17]. Moreover, copper nanoparticles are known to enhance the catalytic activity and selectivity of ZnO in hydration and dehydration reactions, and hydrogenation reactions such as methanol synthesis [18,19]. Copper nanoparticles also play an important role in solid-oxide fuel cells as the active anode material [18,20] and in enhancing the thermal conductivity of fluids [21].

In this paper, copper nanoparticles were synthesized by the solvated metal atom dispersion technique (SMAD) [12,14], and their chemical and catalytic reactivity tested for the Ullman reaction and in the synthesis of methanol over nanocrystals of zinc oxide (NC-ZnO).

* Corresponding author. Tel.: +1 785 532 6849; fax: +1 785 532 6666.
*E-mail address:* kenjk@ksu.edu (K.J. Klabunde).

1381-1169/$ – see front matter © 2004 Elsevier B.V. All rights reserved.
doi:10.1016/j.molcata.2004.08.019

## 2. Experimental

Commercial copper (powder, −200 mesh, 99%) from Aldrich, copper (shot, 2–6 mm, 99.99+%) from Aldrich, toluene (Fisher Scientific, ≥99.5%), diglyme (anhydrous, 99.5%) from Aldrich, THF (Fisher Scientific, ≥99.9%), and pentane (Fisher Scientific, 99%) were used. All the solvents, with the exception of diglyme, were freshly distilled from benzophenone ketal under nitrogen.

The SMAD technique and the apparatus have been described previously [13]. In a typical reaction, 2 g of copper shots were evaporated resistively from a crucible under vacuum and condensed at 77 K with 100 ml of solvent, which was degassed prior to the reaction by taking it through several freeze–thaw–pump cycles. Once deposition was completed, the organic matrix containing the metal was allowed to warm to room temperature; at this point the metal separates from the solvent as a black precipitate at the bottom of the reactor. Thereafter, the solvent is evaporated under dynamic vacuum overnight, and the dried active copper is then removed under argon and placed in the drybox.

### 2.1. Characterization of powders

Differential scanning calorimetric analyses were done using a Perkin-Elmer Pyris-1 DSC under nitrogen. Surface area measurements were carried out in a Micromeretics Flowsorb II 2300 using the Brunauer–Emmet–Teller (BET) method. In this case, the samples were handled under argon all the time and the measurements were taken without previous degassing of the samples in order to avoid sintering. Powder X-ray diffraction (XRD) patterns were taken using a Scintag XRD 3000 diffractometer. For fresh samples, mineral oil was applied in an argon-filled drybox to coat the sample for temporary protection from oxidation by forming a powder/oil paste, since the samples were noticed to react with air when exposed to ambient conditions. The crystallite size was determined from the XRD spectrum using the Scherrer equation.

Transmission electron microscopy (TEM) studies were carried out using a Phillips 201 TEM. The powders were dispersed in dry ethanol followed by sonication of the mix, and then a drop was deposited onto a carbon coated copper grid. Scanning electron microscopy (SEM) studies were carried out in a S-3500N electron microscope from Hitachi Scientific Ltd.; in these cases the samples were passivated previously by exposing them slowly to air.

### 2.2. Chemical reactivity

As mentioned above, the Ullman reaction was the reaction of choice to test the chemical reactivity of our copper samples. In a typical reaction 0.120 g of the active copper was mixed with 0.385 g of phenyl iodide (1:1 molar ratio), a known amount of naphthalene as internal standard (IS), and 3 ml of nonane as solvent. The reaction mixture was heated at 150 °C and 0.1 ml aliquots were taken at different times, each aliquot was filtered and placed in a vial to be later injected in the GC. The 1 μl of the sample was injected in a Varian Star 3600 CX gas chromatograph with a FID detector, and passed through a 30 m long RTX-5 capillary column at a backpressure of 9 psi. In order to separate reactants, products, IS, and solvent from each other, the following temperature set-up was used: kept at 90 °C for 1.5 min and then ramped at 20 °C/min to 170 °C.

The condensation product was characterized using $^1$H NMR and GC–MS. $^1$H NMR spectra were recorded on a 400 MHz Varian spectrometer. Reported chemical shifts refer to room temperature conditions (25 °C). $^1$H NMR chemical shifts were measured relative to tetramethylsilane. GC–MS experiments were carried out on a HP 5890 Series II gas chromatograph with a HP5989A MS detector.

### 2.3. Catalytic reactivity

NC-ZnO was prepared as described in the literature [22]. In order to prepare the samples for the methanol synthesis reaction, 0.7 g of copper was placed in the crucible, 0.7 g of NC-ZnO was placed at the bottom of the SMAD reactor with a Teflon coated stirring bar. The reaction was carried out in the same manner as for the preparation of the copper nanocrystals, with the only difference that as the matrix melted it was kept at −95 °C by immersing the reactor in toluene/liquid-nitrogen slush, stirred for 15 min and allowed to warm to room temperature. Thereafter, the copper coated NC-ZnO ($Cu^*$/NC-ZnO) was dried and handled in the same way as the copper samples.

Elemental analysis of the $Cu^*$/NC-ZnO were conducted by Galbraith Laboratories.

The catalytic activity of our samples was tested in a continuous flow reactor connected to a Varian Star 3600 CX gas chromatograph. In a typical run, 0.1 g $Cu^*$/NC-ZnO was placed between plugs of alumina–silica wool in a Pyrex U-tube contained in a furnace attached to a temperature controller. The length of the bed was between 0.9 and 1.1 cm. The gas mixture (certified gas mixture: 0.99% ethane (as internal standard), 1.97% carbon dioxide, hydrogen balanced) was introduced through one side of the U-tube at 30 ml/min flow rate, and the other side was connected to a 6-port injection valve with a sampling capacity of 1.0 ml. Injections were done every 5 min with the injection valve at 150 °C, and the sample passed through a Porapak Q column at 150 °C with a carrier gas flow of 30 ml/min, and then eluents detected with a TCD detector at 200 °C.

## 3. Results and discussion

### 3.1. Characterization of copper samples

Fig. 1 shows the XRD diffractograms for the freshly prepared samples from different solvents. The peak positions coincide with those of metallic copper with a fcc structure,

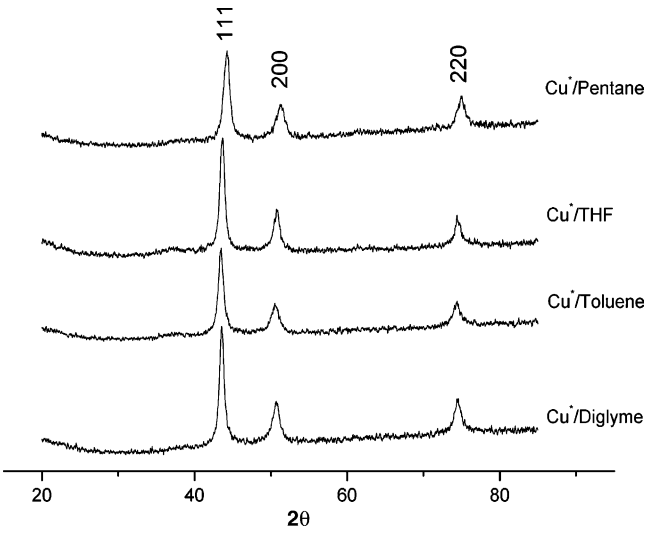


Fig. 1. XRD diffraction patterns of the different copper nanoparticles prepared.

and broadening of the peaks due to crystallites with sizes in the nanometer scale is also observed. The calculated crystallite sizes for the copper samples from peak broadening are listed in Table 1. Peaks corresponding to copper oxide were absent from these spectra, but a small and broad peak around 37° is present in the XRD patterns of passivated samples, suggesting that a layer of copper oxide has been formed on the surface of the particles.

The DSC curves for the freshly prepared samples do not show any thermal event during heating from 25 to 300 °C or cooling to room temperature. On the other hand, passivated samples show an irreversible endothermic peak between 100 and 130 °C attributed to desorption of water adsorbed during passivation; and a broad-irreversible exothermic peak is observed ca. 210 °C attributed to the rearrangement of the atoms on the surface after desorption of water.

TEM images revealed certain similarities between the samples, which present irregular and spherical shaped particles, with an average particle size between 20 and 45 nm (Table 1). The size of our particles are smaller than the 100 nm ones prepared using spray pyrolysis [15], but larger than the 3.6 nm ones prepared by Vitulli et al. [12] using the SMAD method, in this study acetone was used as solvent.

Selected area electron diffraction (SAED) done over the passivated samples reveals four rings corresponding to the lattice planes (1 1 1), (2 0 0), (2 2 0), and (3 1 1), respectively, of the fcc metal copper; and two faint rings that can be attributed to both the lattice planes (1 1 1) and (2 2 0) of copper(I) oxide and to the (−1, 1, 1) and (−1, 1, 3) planes of copper(II) oxide. Similar results were found by Hambrock et al. for ligand-stabilized copper nanoparticles [3]. The above results confirm the presence of an oxide protecting layer on the particles. For the SAED experiments we have taken diffraction patterns for several randomly selective particles of each sample and they all show similar patterns.

A representative TEM image for the passivated samples is shown in Fig. 2. The surface of the samples present agglomerates with sizes in the micrometer range. These agglomerates have a granular structure consisting of agglomerates of the particles observed in the TEM pictures, forming a sponge-like structure.

There are no reports of specific surface areas for copper nanoparticles, except from one estimated from TEM images [12] which is generally not very accurate since neither agglomeration nor the internal structure of the particles was considered. A reasonable explanation for this could be that most of the copper nanoparticles synthesized so far have been ligand-stabilized, which makes them unsuitable for this kind of measurement. The specific surface area for the fresh and passivated samples and the particle size calculated from them [23] are shown in Table 1. The particle size obtained from the specific surface area for three of our samples is smaller than the ones obtained from the TEM images, meaning that they lack porosity. On the other hand, the Cu*/toluene sample seems to posses a modest number of pores, allowing it to adsorb a larger amount of nitrogen. Moreover, since the crystallite size is smaller than the particle size, we can say that our particles are not completely crystalline and that they are constituted by crystalline and amorphous zones. Table 1 also lists the specific surface area and particle size of the commercial sample used in this work. Regarding thermal stability, generally little sintering occurs until about 200 °C for these nanoparticles.

### 3.2. Chemical reactivity

Table 2 summarizes the findings for the homocoupling reaction for our copper samples and the commercial one. The reaction was found to be second order in phenyliodide (Ph-I). When 1/[Ph-I] is plotted versus time, a straight line results. This allowed us to determine the kinetic constant for each reaction from the slope of this line. Moreover, the ratio between the kinetic constant over the specific surface area has been calculated and listed in Table 2 as well. We can say that

Table 1
Properties of the copper samples

| Sample | SSA ($m^2$/g) (fresh samples) | SSA ($m^2$/g) (passivated samples) | Crystallite size (nm) | Particle size from SSA (nm) | Particle size from TEM (nm) |
|---|---|---|---|---|---|
| Cu*/toluene | 27.2 | 27.2 | 8.4 | 29.5 | 20 |
| Cu*/diglyme | 29.6 | 25.4 | 9.9 | 22.7 | 45 |
| Cu*/THF | 29.1 | 28.5 | 9.8 | 23.0 | 35 |
| Cu*/pentane | 23.6 | 20.1 | 12 | 28.6 | 30 |
| Commercial Cu | 0.24 | – | – | 75 μm | – |

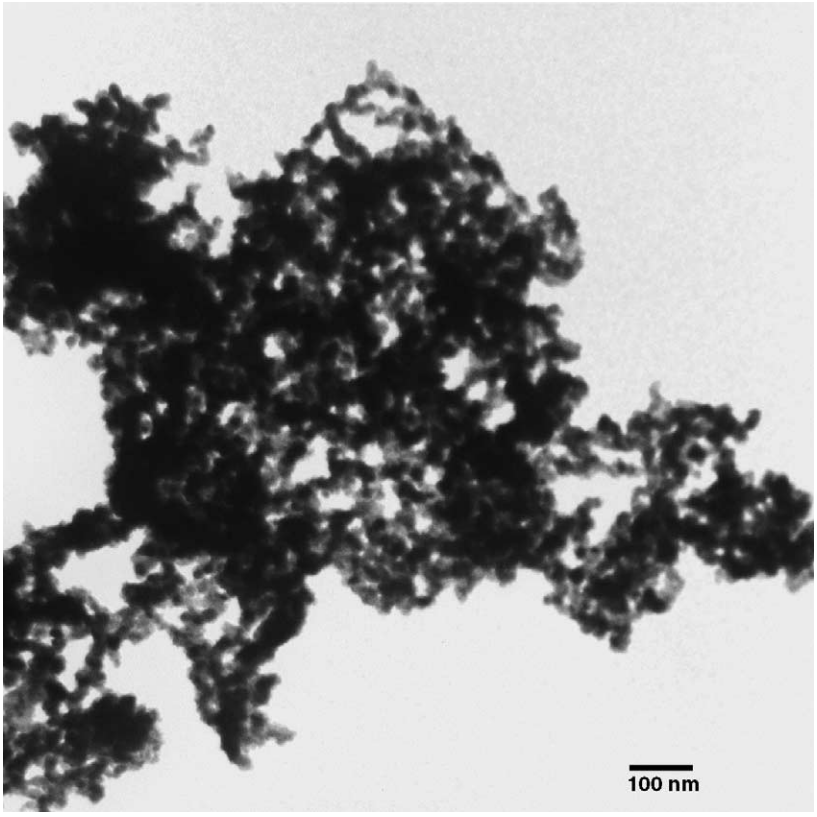


Fig. 2. Representative TEM micrograph of the copper nanoparticles. The Cu*/toluene sample is shown.

the copper samples react with a speed proportional to their surface area, and the order of reactivity observed follows Cu*/toluene > Cu*/THF > Cu*/pentane > Cu*/diglyme. The apparent higher reactivity of the Cu*/toluene sample can be attributed to the smaller particle size and porosity as explained above.

In a typical reaction, the $^1$H NMR of the mixture after reacting for 3 h shows the following peaks for iodobenzene: $\delta$ 7.73, d (2H); 7.36, m (1H); 7.13, t (2H); and for diphenyl: $\delta$ 7.71, d (4H); 7.47, t (4H); 7.38, m (2H). In the chromatograms, a small unknown peak with a short retention time is obtained. This peak comes from benzene produced during the reaction, and gave rise to a molecular ion at $m/z$ = 78 in the MS spectrum.

Table 3 shows experimental conditions and results found in the literature for different copper samples. Comparing our samples, we can state that our samples are more reactive, considering that the copper nanoparticles have been

Table 2
Reaction conditions and results for the Ullman reaction in this work

| Sample | $K$ ($s^{-1}$) | $K$/SSA | Reaction time (h) | Molar ratio, Cu:Ph-I | Yield of biphenyl (%) |
|---|---|---|---|---|---|
| Cu*/toluene | 0.026 | 9.6E−4 | 6 | 1:1 | 89 |
| Cu*/diglyme | 0.003 | 1.0E−4 | 6 | 1:1 | 52 |
| Cu*/THF | 0.010 | 3.5E−4 | 6 | 1:1 | 80 |
| Cu*/pentane | 0.005 | 2.1E−4 | 6 | 1:1 | 70 |
| Commercial Cu | 2E−4 | 8.3E−4 | 6 | 1:1 | 35 |

All reactions were carried out at 150 °C.

Table 3
Reaction conditions and results for the Ullman reaction from the literature

| Kind of sample | Particle size (nm) | Reaction temperature (°C) | Reaction time (h) | Yield of biphenyl (%) | Molar ratio, Cu:Ph-I | Reference |
|---|---|---|---|---|---|---|
| Sonochemical reduction (powder) | 50–70 | 200 | 5 | 88 | 1.6:1 | [2] |
| Thermal reduction (powder) | 200–250 | 200 | 5 | 79 | 1.6:1 | [2] |
| Commercial | 500–600 | 200 | 5 | 43 | 1.6:1 | [2] |
| Chemical reduction (colloid) | – | 85 | 24 | 66 | 2:1 | [5,6] |

Table 4
Specific surface area of the Cu*/NC-ZnO samples

| Sample | SSA ($m^2$/g) |
|---|---|
| Cu*/toluene/NC-ZnO | 57 |
| Cu*/diglyme/NC-ZnO | 12 |
| Cu*/THF/NC-ZnO | 48 |
| Cu*/pentane/NC-ZnO | 54 |

mixed with iodobenzene in a lower molar ratio and that the reaction temperature is either lower or the reaction time shorter.

### 3.3. Characterization of Cu*/NC-ZnO

The NC-ZnO prepared using a modified sol–gel procedure posses a crystallite size of 3–5 nm, an average surface area of 120 $m^2$/g, and they agglomerate into large spherical particles with an average diameter of 260 nm [22]. The surface area of our NC-ZnO sample was 95 $m^2$/g, which is lower than that reported in literature; the cause for this could be due to the fact that our sample was not degassed before the surface area was measured. The surface areas obtained for the Cu*/NC-ZnO after passivation are listed in Table 4. As we can see the total surface area is much lower, which is attributed to the closing of pore openings by the copper particles. Surprisingly, Cu*/diglyme/NC-ZnO shows a surface area which is even smaller than for the Cu*/diglyme sample, and this was also observed (11.5 $m^2$/g) for a sample from a different batch. We can explain this based in the fact that the NC-ZnO is a very porous material and could have absorbed a certain amount of solvent in its interior, which was not entirely removed during the drying due to its high boiling point (162 °C).

The elemental analysis of the Cu*/NC-ZnO is shown in Table 5. These values translate into an empirical formula of $Cu_{0.70}Zn_{0.52}C_{0.058}H_{0.60}O_{1.25}$, so it is evident that both metals exist as oxides. The carbon and hydrogen is probably due to solvents fragments present. In the case of Cu*/diglyme/NC-ZnO the amount of carbon is surprisingly large compared to the other samples, and this corroborates the presence of some solvent in the sample as stated earlier for the unusually low surface area of the sample.

The XRD diffractograms of the samples do not show any crystalline copper, and this is expected due to the low density of the sample and low volume concentration of the copper.

Fig. 3 shows a typical TEM micrograph of the Cu*/NC-ZnO samples. The images show that the copper nanoparticles completely cover the porous, larger ZnO nanostructured spheres.


Fig. 3. Representative TEM micrograph of the Cu*/NC-ZnO.

### 3.4. Catalytic activity

For the first time two different nanoscale materials prepared in our laboratories, have been combined in an attempt to enhanced catalytic activity. The reaction was studied from room temperature to 450 °C and maximum conversion calculated at its steady state.

Fig. 4 shows the conversion of $CO_2$ to methanol as a function of the temperature of our samples compared with NC-ZnO and NC-ZnO/CuO from Ref. [23]. The conversion increases as temperature rises, and the maximum conversion is attained at 450 °C. Notice that the Cu*/NC-ZnO samples became progressively more active and are clearly superior at the higher temperature. For the NC-ZnO/CuO sample, the change in the conversion rate could be due to the reduction of the copper oxide; once completed it proceeds at higher conversion rate. Furthermore, all of our samples show higher conversion than NC-ZnO and NC-ZnO/CuO at 450 °C, and this, indicates that copper nanocrystals on the surface of NC-

Table 5
Elemental analysis of the Cu*/NC-ZnO samples

| | Cu*/toluene/NC-ZnO | Cu*/diglyme/NC-ZnO | Cu*/THF/NC-ZnO | Cu*/pentane/NC-ZnO |
|---|---|---|---|---|
| Copper | 44.9 | 40.6 | 45.6 | 49.5 |
| Zinc | 34.4 | 37.7 | 30.8 | 33.4 |
| Carbon | 0.70 | 2.8 | 0.75 | 0.78 |
| Hydrogen | 0.63 | 0.57 | 0.63 | 0.65 |

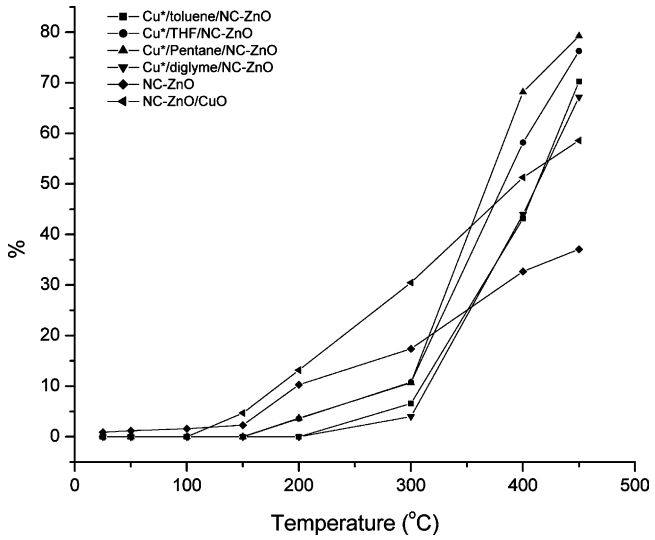


Fig. 4. The percentage of $CO_2$ converted to $CH_3OH$ vs. temperature for the $Cu^*$/NC-ZnO samples from this work, and for NC-ZnO and NC-ZnO/CuO from Ref. [23].

ZnO yield the best catalytic formulation. Also, since CO is an intermediate product, the higher temperature and the presence of copper metal nanoparticles could help explain the higher conversion rates.

The reaction reaches its steady state during the first 50 min. In order to determine the conversion of $CO_2$ to methanol, the samples were allowed to react for 2 h at 450 °C, and then average conversion calculated from the chromatograms obtained after injecting every 15 min for a period of 3 h. The results showed the following, percentage $CO_2$ converted to $CH_3OH$: NC-ZnO (37%), NC-Zn/CuO (59%), $Cu^*$/toluene/NC-ZnO (68%), $Cu^*$/diglyme/NC-ZnO (74%), Cu/THF/NC-ZnO (76%), and $Cu^*$/pentane/NC-ZnO (80%), all with a 0.3 s contact time.

## 4. Conclusions

We have successfully prepared copper nanoparticles with an average diameter of 20–45 nm and a surface area of 24–30 $m^2$/g containing crystallite sizes of 8–12 nm. These particles, when slowly exposed to air, display a core-shell structure formed by a metallic core encapsulated by a layer of amorphous copper oxide. Their chemical reactivity in the Ullman reaction is proportional to their surface area, and more reactive than those found in literature. The order of reactivity for the solvents used in the preparation of the active copper are as follows: $Cu^*$/toluene > $Cu^*$/THF > $Cu^*$/pentane > $Cu^*$/diglyme, with a maximum yield of 90% biphenyl at 150 °C after 6 h for the $Cu^*$/toluene sample (all the reactions were carried out in nonane solvent).

Preparation of $Cu^*$/NC-ZnO samples results in a reduction of the surface area of the NC-ZnO due to clogging of pore openings by the copper particles. Substantial absorption of solvent by the NC-ZnO is observed especially for the $Cu^*$/diglyme/NC-ZnO sample. This solvent absorption plays an important role during the catalytic experiments of hydrogenation of $CO_2$ to form $CH_3OH$, by slowing down the kinetics of the reaction and increasing the temperature at which methanol starts being produced.

The $Cu^*$/NC-ZnO samples show a larger conversion of $CO_2$ to methanol at 450 °C compared with NC-ZnO and NC-ZnO/CuO, and a maximum conversion of 80% was obtained for the $Cu^*$/pentane/NC-ZnO sample.

## Acknowledgement

The support of the National Science Foundation is acknowledged with gratitude.

## References

[1] K.J. Klabunde, Nanoscale Materials in Chemistry, Wiley/Interscience, New York, 2001.
[2] N.A. Dhas, C.P. Raj, A. Gedanken, Chem. Mater. 10 (1998) 1446–1452.
[3] J. Hambrock, R. Becker, A. Birkner, J. Weiß, R. Fischer, Chem. Commun. (2002) 68–69.
[4] R.A. Salkar, P. Jeevanandam, G. Kataby, S.T. Aruna, Y. Koltypin, O. Palchik, A. Gedanken, J. Phys. Chem. B 104 (2000) 893–897.
[5] G.W. Ebert, R.D. Rieke, J. Org. Chem. 49 (1984) 5280–5282.
[6] G.W. Ebert, R.D. Rieke, J. Org. Chem. 53 (1988) 4482–4488.
[7] H.H. Huang, F.Q. Yan, Y.M. Kek, C.H. Chew, G.Q. Xu, W. Ji, P.S. Oh, S.H. Tang, Langmuir 13 (1997) 172–175.
[8] F. Bonet, S. Grugeon, L. Dupont, R. Herrera Urbina, C. Guery, J.M. Tarascon, J. Solid State Chem. 172 (1) (2003) 111–115.
[9] J. Tanori, M.P. Pileni, Adv. Mater. 7 (10) (1995) 862–864.
[10] A. Henglein, J. Phys. Chem. B 104 (2000) 1206–1211.
[11] T. Chen, S. Chen, H. Sheu, C. Yeh, J. Phys. Chem. B 106 (2002) 9717–9722.
[12] G. Vitulli, M. Bernini, S. Bertozzi, E. Pitzalis, P. Salvadori, S. Coluccia, G. Martra, Chem. Mater. 14 (2002) 1183–1186.
[13] K.J. Klabunde, P.S. Timms, P.S. Skell, S. Ittel, Inorg. Synth. 19 (1979) 59.
[14] S.C. Davis, K.J. Klabunde, Chem. Rev. 82 (1982) 153–208.
[15] J.H. Kim, T.A. Germer, G.W. Mulholland, S.H. Ehrman, Adv. Mater. 14 (7) (2002) 518–521.
[16] R.D. Rieke, R.M. Wehmeyer, T.C. Wu, G.W. Ebert, Tetrahedron 45 (1989) 443.
[17] J. Hassan, M. Sévignon, C. Gozzi, E. Schulz, M. Lemaire, Chem. Rev. 102 (2002) 1359–1469.
[18] S. Park, R.J. Gorte, J.M. Vohs, Appl. Catal. A 200 (2000) 55.
[19] M. Twigg, Catalysis Handbook, 2nd ed., Wolfe Publishing Ltd., 1989.
[20] R.J. Gorte, Adv. Mater. 12 (2000) 1465;
S. Park, Nature 404 (2000) 265.
[21] J.A. Eastman, S.U.S. Choi, S. Li, W. Yu, L.J. Thompson, Appl. Phys. Lett. 78 (6) (2001) 718–720.
[22] C.L. Carnes, K.J. Klabunde, Langmuir 16 (2000) 3764–3772.
[23] C.L. Carnes, K.J. Klabunde, J. Mol. Catal. 194 (2003) 227–236.